Supplement Materials for

Strategic Design of Methane Observation Networks to Improve Emission Estimates: A Case Study in Africa

Hui Li[1]*, Philippe Ciais[1], Frédéric Chevallier[1], Bo Zheng[2,3], Paul I. Palmer[4], Frank Hase[5], Morgan Lopez[1], Elsa M Ordway[6], Shushi Peng[7], Danielle Monteverde[8], Michel Ramonet[1], Jason Michael St Clair[9], Le Bienfaiteur Sagang[10], Benjamin Poulter[11]

[1]Laboratoire des Sciences du Climat et de l'Environnement, LSCE/IPSL, CEA-CNRS-UVSQ, Université Paris-Saclay, F-91191 Gif-sur-Yvette, France.

[2]Shenzhen Key Laboratory of Ecological Remediation and Carbon Sequestration, Institute of Environment and Ecology, Tsinghua Shenzhen International Graduate School, Tsinghua University, Shenzhen 518055, China.

[3]State Environmental Protection Key Laboratory of Sources and Control of Air Pollution Complex, Beijing 100084, China.

[4]National Centre for Earth Observation, University of Edinburgh, Edinburgh, EH9 3FF, UK.

[5]Institute of Meteorology and Climate Research (IMK-ASF), Karlsruhe Institute of Technology (KIT), 76344 Eggenstein-Leopoldshafen, Germany.

[6]Department of Ecology and Evolutionary Biology and Institute of the Environment and Sustainability, University of California, Los Angeles, Los Angeles, California, USA.

[7]Institute of Carbon Neutrality, Sino-French Institute for Earth System Science, College of Urban and Environmental Sciences, and Laboratory for Earth Surface Processes, Peking University, Beijing, China.

[8]Spark Climate Solutions, Covina, CA, 91723, USA.

[9]NASA Goddard Space Flight Center, Greenbelt, MD, USA.

[10]Institute of the Environment and Sustainability, University of California, Los Angeles, Los Angeles, CA, USA.

[11]Spark Climate Solutions, San Francisco, CA, USA.

Correspondence to: Hui Li (hui.li@lsce.ipsl.fr)

This file includes:

Figures S1-S12

Tables S1-S5

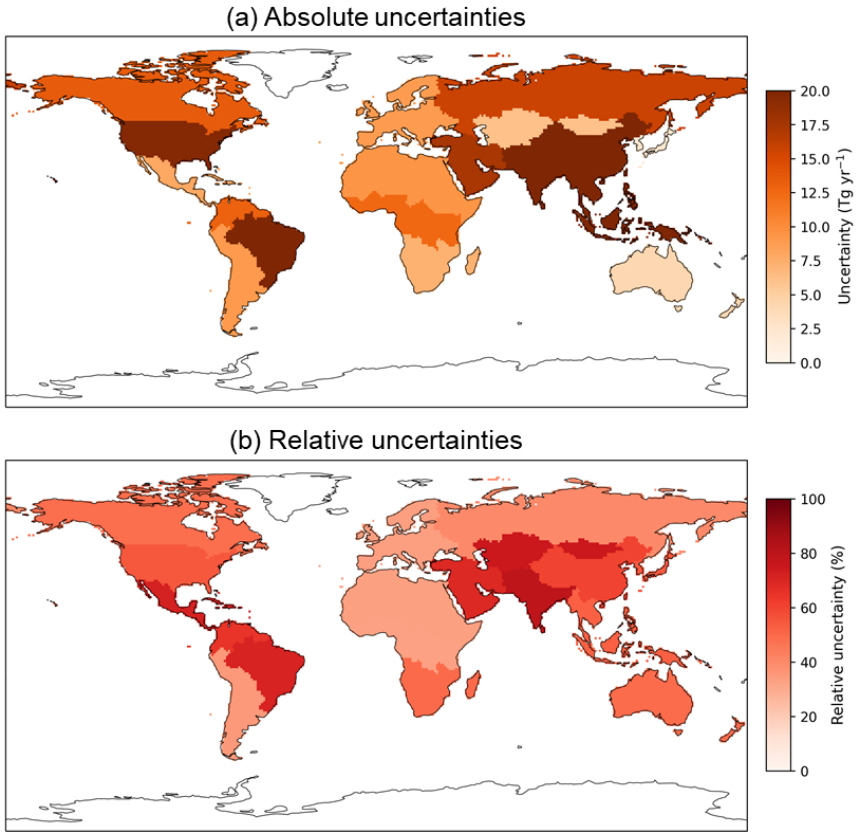

Figure S1. Regional annual prior uncertainty budget for CH_4 emissions derived from the prior error covariance matrix B used in this study. The uncertainty for each region is calculated as $\sigma^2=\mathbf{l}^T\mathbf{B}\mathbf{l}$, where $\mathbf{l}$ represents the vector converting grid-scale emissions into regional totals. The upper panel shows the absolute annual uncertainty (Tg yr^{-1}), and the lower panel shows the corresponding relative uncertainty (%), defined as the ratio of the uncertainty to the regional annual prior emissions.

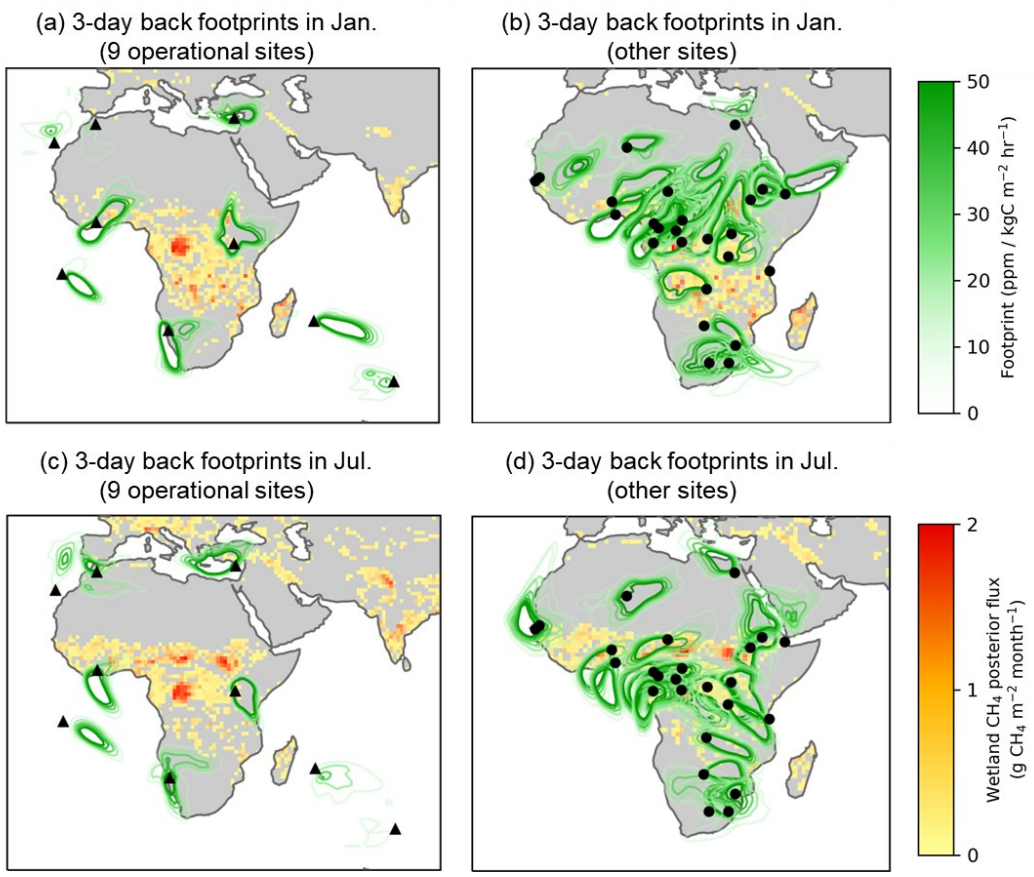

Figure S2. Spatial distribution of 3-day backward transport footprints over Africa for January (top row) and July (bottom row). (a) and (c) show footprints associated with the 9 operational sites, while (b) and (d) correspond to other 25 sites. Green contours represent footprint sensitivities (ppm kgC m^{-2} hr^{-1}), indicating the influence of surface methane emissions on the column observations. The background shows wetland CH_4 emissions (g CH_4 m^{-2} $month^{-1}$), emissions less than 0.05 g CH_4 m^{-2} $month^{-1}$ are gray-shaded for clarity. Black dots (triangles and circles) denote the locations of surface observation sites.

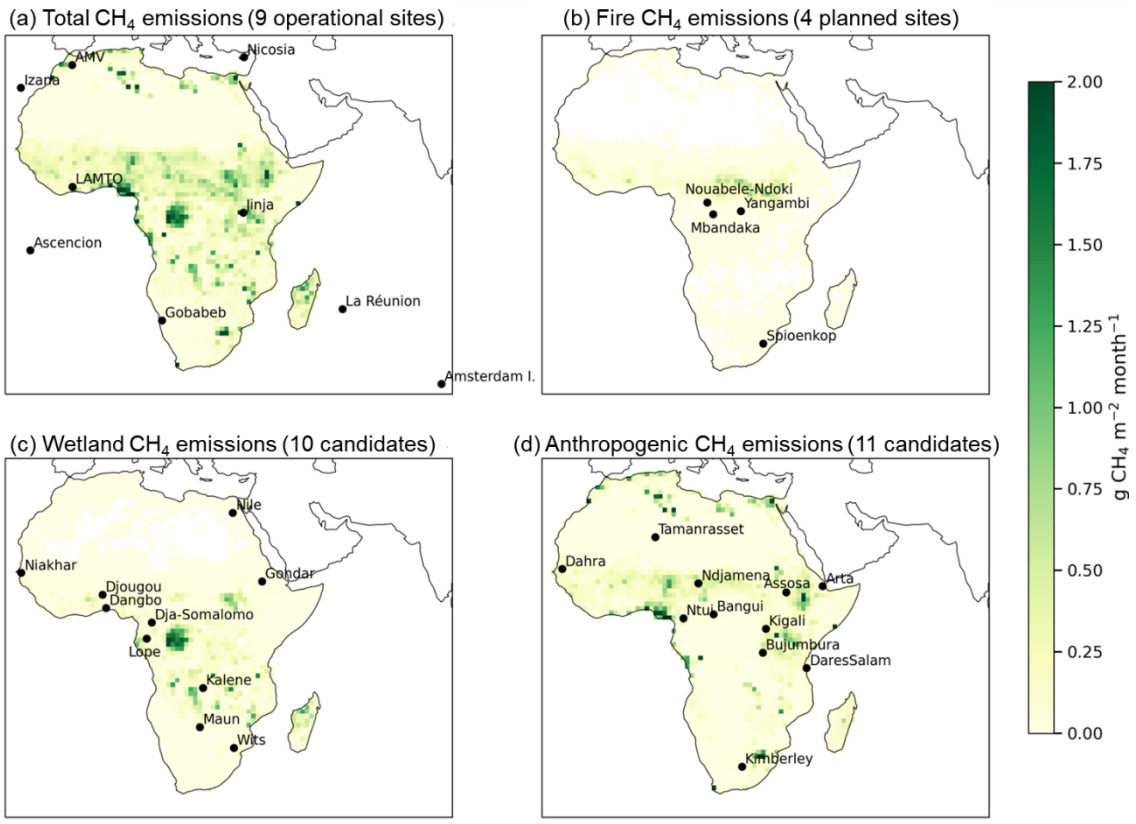

Figure S3. Sectoral CH_4 emissions and observation coverage over Africa in January. (a) total CH_4 emissions with current 9 operational sites (La Réunion, Nicosia, Ascension, Izaña, LAMTO, AMV, Gobabeb, Jinja, Amsterdam Island); (b) fire CH_4 emissions with 4 planned observation sites (Yangambi, Mbandaka, Nouabele-Ndoki, Spioenkop); (c) wetland CH_4 emissions with 10 candidate sites (Dja-Somalomo, Wits, Niakhar, Nile, Djougou, Dangbo, Kalene, Gondar, Lope, Maun); and (d) anthropogenic CH_4 emissions with the remaining 11 candidate sites (Dahra, Ntui, Kigali, Bujumbura, Arta, Assosa, Bangui, Kimberley, Tamanrasset, Ndjamena, DaresSalam).

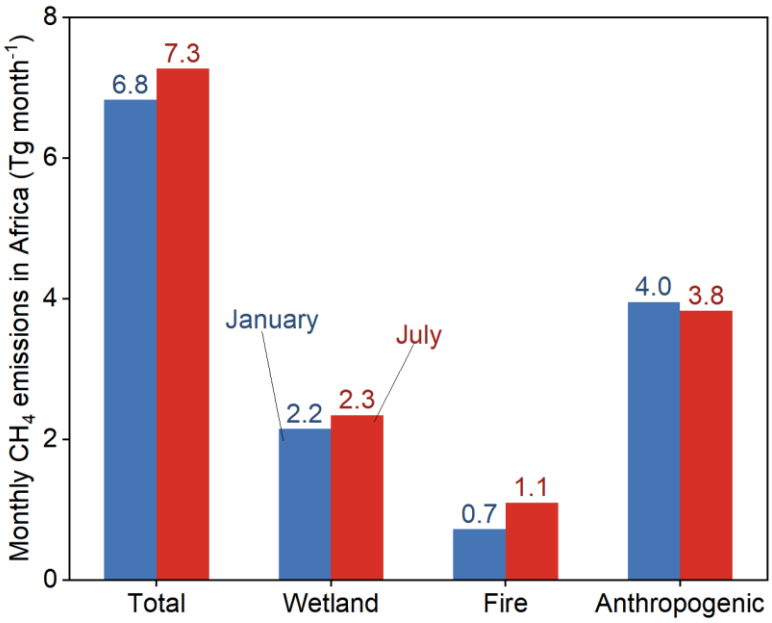

Figure S4. Comparison of African CH_4 emissions across sectors between January and July in 2023.

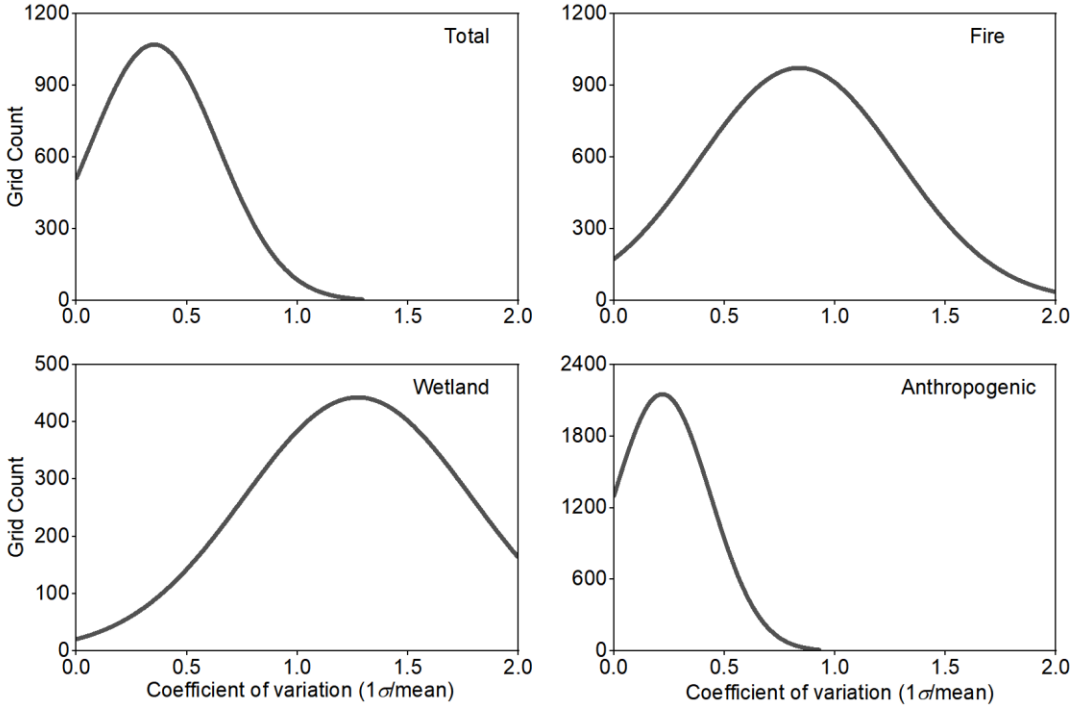

Figure S5. The coefficient of variation for sectoral CH_4 prior emissions adopted in this study.

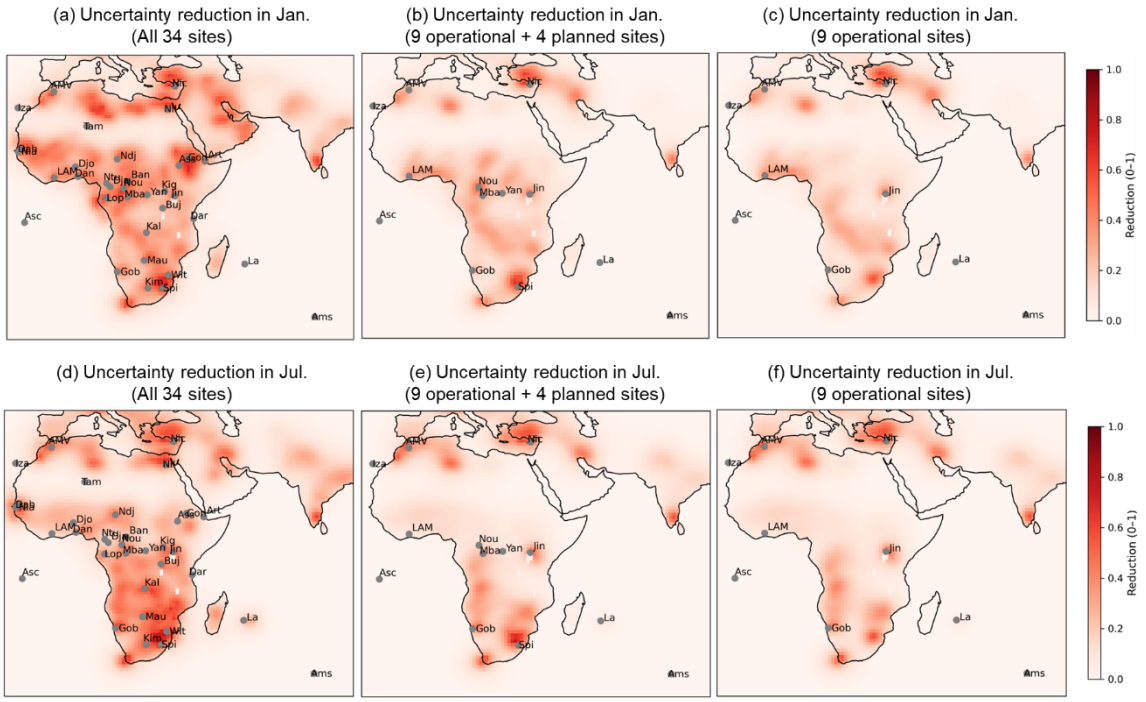

Figure S6. Spatial distribution of uncertainty reduction for total CH_4 emissions under different site deployments and months.

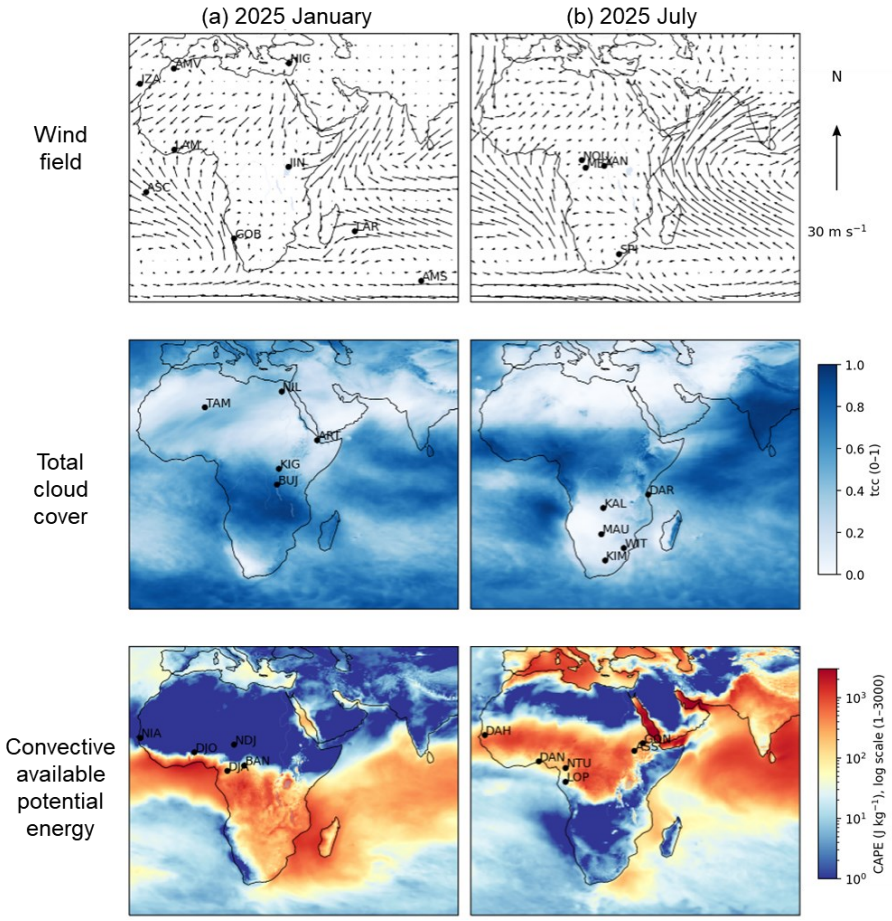

Figure S7. Meteorological conditions over Africa in January (left column) and July (right column) 2025. The top row shows 10-m wind fields, the middle row presents total cloud cover (TCC), and the bottom row displays convective available potential energy (CAPE). Black dots indicate 34 sites listed in Table S2, with their first three letters for clarity here. Data are from ERA5 dataset (https://cds.climate.copernicus.eu/datasets).

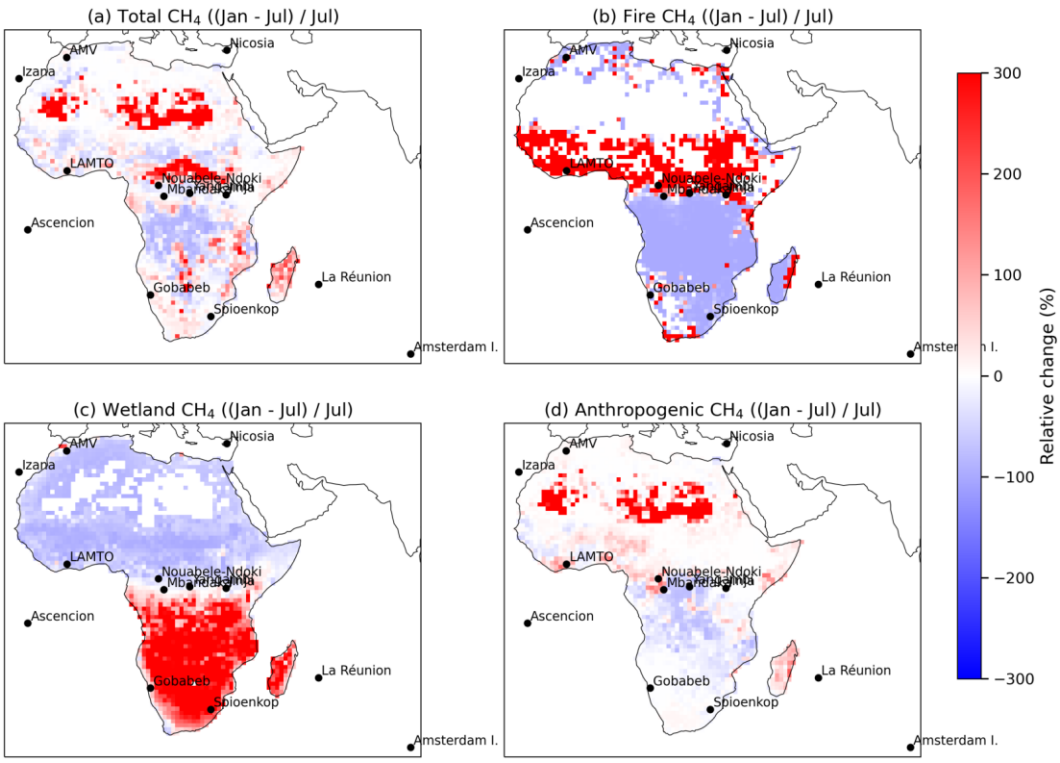

76

77 **Figure S8. Spatial difference between January and July for (a) total; (b) fire; (c) wetland; and**
78 **(d) anthropogenic CH_4 emissions.** Here presents the relative difference calculated as (January -
79 July)/July. Dots denote 9 operational and 4 planned sites.

80

81

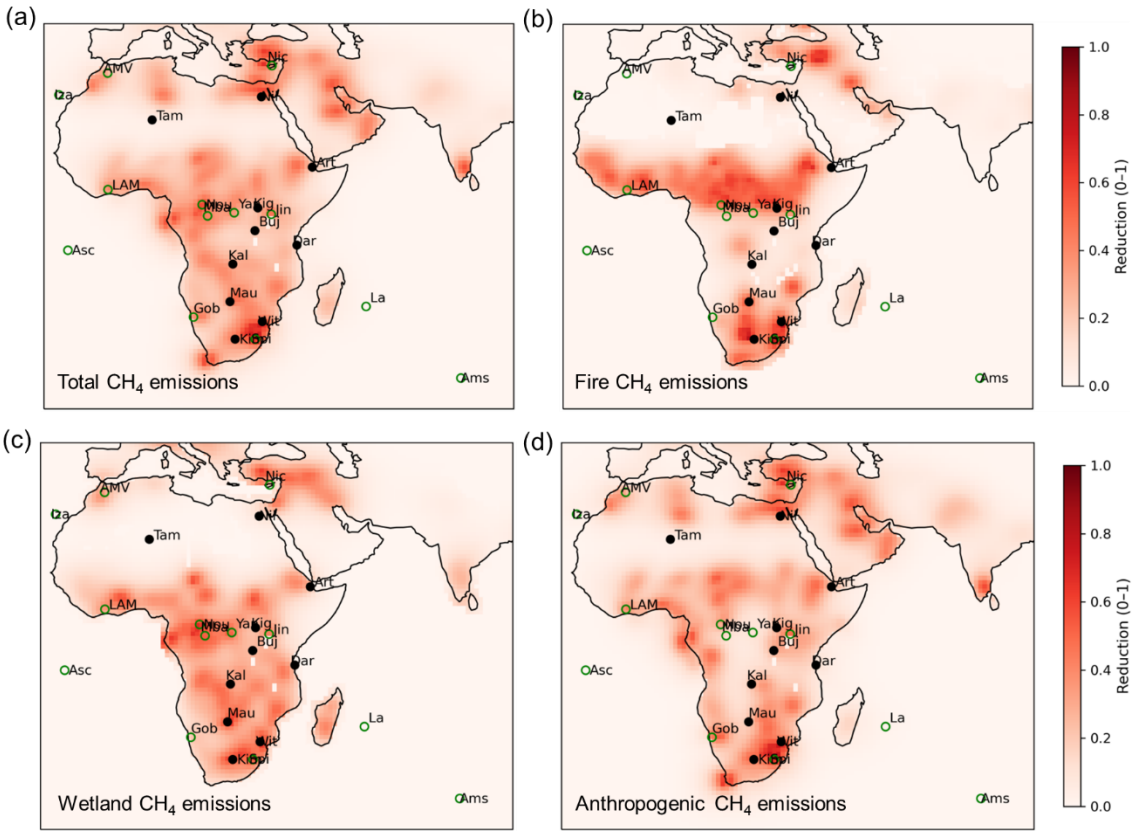

Figure S9. Spatial distribution of uncertainty reduction for (a) total; (b) fire; (c) wetland; and (d) anthropogenic CH_4 emissions with the 10 optimal sites configuration in 2025 January. The 10 optimal sites in this case include Nile, Tamanrasset, Arta, Kigali, Bujumbura, DaresSalam, Kalene, Maun, Wits, and Kimberley. All the site names are abbreviated with first three letters. The green open circles are 9 operational and 4 planned sites, and the closed black circles are optimized new 10 sites.

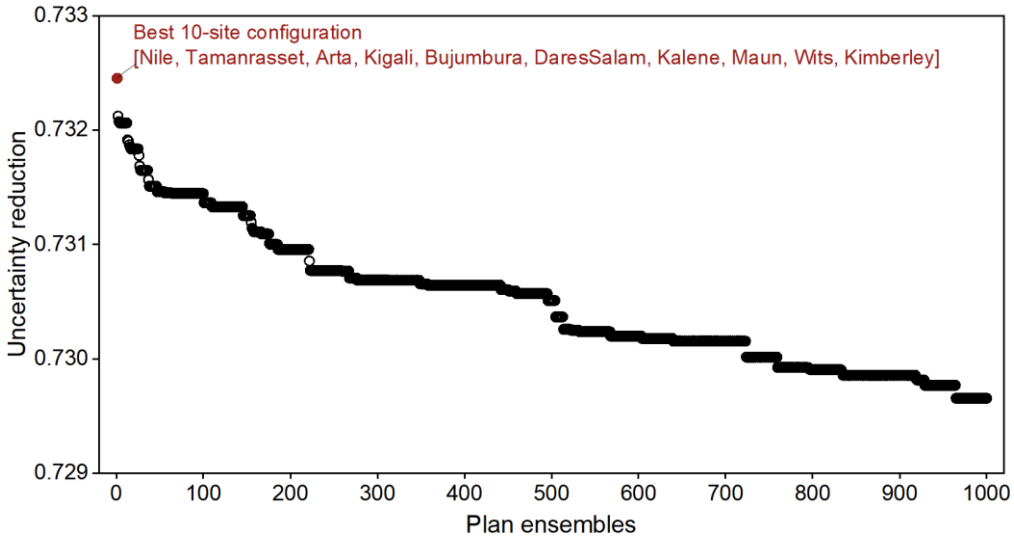

Figure S10. The best site configuration selection among 10-site plans (top 1000 plans are plotted).

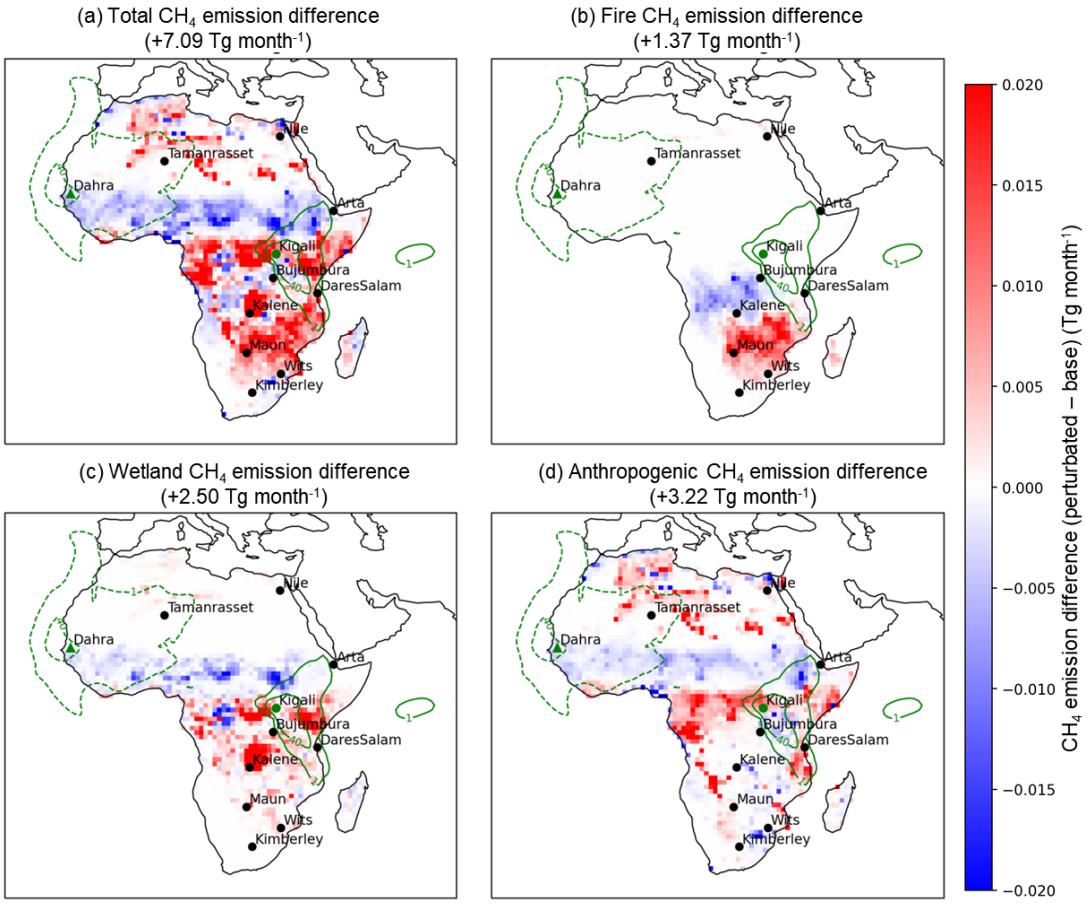

Figure S11. Spatial differences in July CH_4 prior emissions between the perturbed prior and the base prior over Africa. Panels show (a) total, (b) fire, (c) wetland, and (d) anthropogenic CH_4. Colors denote the grid-cell emission difference (perturbed-base). Black markers indicate optimal selected sites common to both priors, green circles indicate sites included only in base prior (Kigali), and green triangles indicate sites included only in perturbed prior test (Dahra). Green contour lines overlay the 3-day footprints for sites unique to each condition (solid for base prior; dashed for perturbed prior test), with numbers denoting the corresponding footprint values.

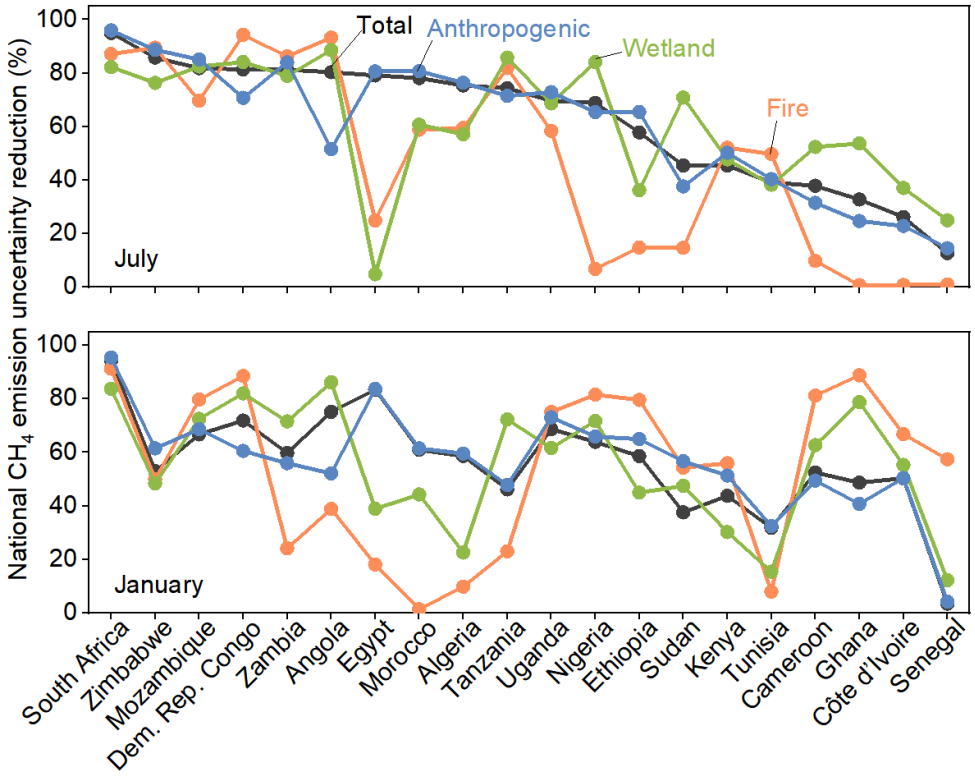

105

106 **Figure S12. Country-specific CH_4 emission uncertainty reduction with the 10 optimal site**
107 **configurations.** Only 20 countries are presented here for clarity, with more country results listed
108 in Table S5.

109

Table S1. The database used as CH_4 priors in 2023 in this study.

Sectors	Database	Source
Fire	GFEDv4	https://www.globalfiredata.org/
	GFEDv5	
	GFAS	https://ads.atmosphere.copernicus.eu/datasets/cams-global-fire-emissions-gfas?tab=overview
Wetland	ORCHIDEE	Peng et al. (2022) and Liu et al. (2025)
	LPJ-EOSIM	Ciais et al. (2026)
	DLEM	
	FLUXNET-CH_4	
Anthropogenic	CEDS v2025_04_18	https://github.com/JGCRI/CEDS
	EDGAR v2024	https://edgar.jrc.ec.europa.eu/emissions_data_and_maps
	EDGAR v2025	
Total	Sum of anthropogenic and natural sources	

Table S2. The XCH_4 site pool in Africa in this study, with spatial distribution presented in Fig. 3.

Country	Site	Lat	Lon	Status
France	La Réunion[#]	-21.0833	55.3917	Operational FTIR sites · ([#]are sites within TCCON network) · ([*]are sites operated by the Laboratory for Climate and Environmental Sciences) · (Gobabeb is operated by the Karlsruhe Institute of Technology) · (Jinja is operated by the University of Leicester)
Cyprus	Nicosia[#]	35.1410	33.3800	
UK	Ascencion[#]	-7.9667	-14.4000	
Spain	Izaña[#]	28.3090	-16.4990	
Côte d'Ivoire	LAMTO[*]	6.2244	-5.0278	
Maroc	AMV[*]	33.4062	-5.1033	
France	Amsterdam I.[*]	-37.7976	77.5725	
Namibia	Gobabeb	-23.5622	15.0409	
Uganda	Jinja	0.4165	33.2070	
Congo	Yangambi	0.8100	24.5000	Planned sites
Congo	Mbandaka	0.0500	18.3000	
Dem. Rep. Congo	Nouabele-Ndoki	2.7000	17.0000	
South Africa	Spioenkop	-28.7132	29.5086	
Cameroon	Dja-Somalomo	3.3738	12.7331	Candidates
Algeria	Tamanrasset	22.47	5.31	
Chad	Ndjamena	12.1265	14.9997	
Tanzania	DaresSalam	-6.7808	39.20369	
Cameroon	Ntui	4.4000	11.6200	
Senegal	Niakhar	14.5000	-16.4000	
Senegal	Dahra	15.3600	-15.4800	
Benin	Djougou	9.6500	1.7333	
Benin	Dangbo	6.6014	2.5465	
Ethiopia	Assosa	10.1000	34.6000	
Ethiopia	Gondar	12.6000	37.4500	
Djibouti	Arta	11.5000	42.8000	
Rwanda	Kigali	1.9617	30.0642	
Botswana	Maun	-19.9022	23.5283	
Egypt	Nile	27.8800	30.8900	
Burundi	Bujumbura	-3.3600	29.3700	
Zambia	Kalene	-11.1755	24.1917	
Gabon	Lope	-0.2000	11.6000	
Central African Rep.	Bangui	5.2000	18.4000	
South Africa	Kimberley	-28.7300	24.7540	
South Africa	Wits	-24.5530	31.0970	

Table S3. The parameter settings in the site-design system.

	Parameters	Default	Definition and description
General settings	MONTH	01/07	- Target month for the optimization. All calculations are performed independently for each month to account for seasonal variability in emissions, transport, cloud cover, and observational sensitivity.
	σ_obs	5 ppb	- Assumed observational uncertainty for each site and valid day.
Cloud screening	Cloud fraction (CF) threshold	0.5	- ERA5 cloud fraction threshold applied to filter out days with excessive cloud cover, reducing effective observational sensitivity.
	Minimum valid fraction	0.1	- Minimum fraction of cloud-free days required for a site to be considered active within a given month.
Optimization of the number of additional sites and site configuration	ε	0.6%	- Threshold for the marginal gain in ensemble-mean uncertainty reduction. The optimal number of additional sites n^* is defined as the smallest n for which the incremental relative reduction $\Delta P(n)$ falls below ε, indicating diminishing returns from further network expansion.
	$\boldsymbol{B}$ (Sector-specific)	-	- For sectoral uncertainty reduction, the prior covariance matrix **B** is modified to reflect sector-specific uncertainties, while the transport sensitivity matrix **H** is assumed to be identical to that for total emissions.

Table S4. The sensitivity tests on parameters.

Parameters		Test Name	Test Value	Optimal Site Number (10)	Optimal Site Configuration [Arta, Bujumbura, DaresSalam, Kalene, Kigali, Kimberley, Maun, Nile, Tamanrasset, Wits]
Observation uncertainty (ppb) (5)		R1	1	10	- [Arta, Bujumbura, DaresSalam, Kalene, Kigali, Kimberley, Maun, Nile, Tamanrasset, Wit]
		R10	10	10	- [Arta, Bujumbura, DaresSalam, Kalene, Kigali, Kimberley, Maun, Nile, Tamanrasset, Wit]
		R100	100	12	- [Arta, Bujumbura, Dahra, DaresSalam, Kalene, Kigali, Kimberley, Maun, Niakhar, Nile, Tamanrasset, Wits]
		R1000	1000	21	- All candidates
Cloud effect	Cloud fraction (0.5)	CF0.3	0.3	19	- [Arta, Assosa, Bangui, Bujumbura, Dahra, Dangbo, DaresSalam, Dja-Somalomo, Kalene, Kigali, Kimberley, Lope, Maun, Ndjamena, Niakhar, Nile, Ntui, Tamanrasset, Wits]
		CF0.4	0.4	13	- [Arta, Bangui, Bujumbura, Dahra, Dangbo, Kalene, Kigali, Kimberley, Maun, Niakhar, Nile, Tamanrasset, Wits]
		CF0.6	0.6	2	- [DaresSalam, Nile]
		CF0.7	0.7	2	- [Arta, DaresSalam]
	Minimum valid fraction (0.1)	VF0	0	13	- [Arta, Assosa, Bujumbura, Dahra, Dja-Somalomo, Kalene, Kigali, Kimberley, Maun, Niakhar, Nile, Ntui, Wits]
		VF0.2	0.2	4	- [DaresSalam, Kalene, Maun, Nile]
		VF0.3	0.3	1	- [DaresSalam]
		VF0.4	0.4	1	- [DaresSalam]
System Parameter	ε (0.6%)	ε_0.5%	0.5%	14	- [Arta, Bujumbura, Dahra, DaresSalam, Dja-Somalomo, Kalene, Kigali, Kimberley, Lope, Maun, Niakhar, Nile, Tamanrasset, Wits]
		ε_0.7%	0.7%	7	- [Bujumbura, DaresSalam, Kalene, Kimberley, Maun, Nile, Wits]

* The numbers below each parameter are the corresponding default values.

Table S5. National CH_4 uncertainty reduction (%) with ten optimal site configurations.

Country list	July				Jan			
	Total	Fire	Wetland	Anthropogenic	Total	Fire	Wetland	Anthropogenic
Angola	80	93	89	52	75	39	86	52
Algeria	75	60	57	76	59	10	23	60
South Africa	95	87	82	96	94	91	84	95
Zimbabwe	86	90	76	89	53	50	48	61
Mozambique	82	70	82	85	67	80	72	69
Dem. Rep. Congo	81	94	84	71	72	89	82	61
Zambia	81	86	79	84	60	24	72	56
Madagascar	52	56	61	58	34	21	54	21
Tanzania	74	82	86	71	46	23	72	48
Gambia	9	1	18	10	2	41	8	2
Botswana	84	92	84	83	65	85	78	65
Egypt	79	25	5	81	83	18	39	84
Senegal	13	1	25	15	3	57	12	4
S. Sudan	47	12	76	25	64	88	83	43
Namibia	83	80	69	88	54	34	56	61
Guinea-Bissau	11	1	19	12	2	40	9	3
Congo	65	74	77	56	72	55	83	59
Morocco	78	59	61	81	61	1	44	61
Libya	41	8	4	45	38	29	3	44
Chad	60	19	73	60	75	86	76	83
Sudan	45	15	71	38	38	54	47	57
Mali	42	3	52	42	27	58	26	32
Malawi	64	47	62	70	49	48	54	49
Lesotho	62	72	48	64	55	54	51	57
Eswatini	63	63	60	64	57	63	51	58
Uganda	70	58	69	73	69	75	62	73
Guinea	32	1	46	31	11	80	31	9
Burkina Faso	40	2	54	33	34	40	29	41
Nigeria	69	7	84	65	64	82	72	66
Rwanda	49	53	43	53	28	20	30	37
Niger	40	12	48	39	29	30	22	39
Burundi	52	61	37	61	23	12	29	33
Central African Rep.	45	12	67	26	53	89	59	56
Benin	37	1	43	39	50	44	41	51
Mauritania	14	1	26	16	5	32	11	6
Ghana	33	1	54	25	49	89	79	41
Cameroon	38	10	52	31	52	81	63	49
Kenya	45	52	48	50	44	56	30	51
Togo	31	1	40	30	42	53	52	39
Ethiopia	58	15	36	66	59	80	45	65
Tunisia	39	50	38	40	32	8	15	32
Sierra Leone	17	1	23	17	6	41	15	5
Côte d'Ivoire	26	1	37	23	50	67	55	50
Gabon	51	41	67	43	70	20	82	64
Liberia	15	0	21	15	12	51	22	10
Eritrea	20	18	16	25	28	41	30	29
Eq. Guinea	27	4	21	33	38	14	35	42
Djibouti	11	13	9	13	25	22	32	26
Somaliland	7	6	4	7	12	10	9	13
W. Sahara	4	-	3	4	3	-	3	3
Somalia	4	3	4	5	17	4	5	28

References

Ciais, P., Zhu, Y., Cai, Y., Lan, X., Michel, S. E., Zheng, B., Zhao, Y., Hauglustaine, D. A., Lin, X., Zhang, Y., Sun, S., Tian, X., Zhao, M., Wang, Y., Chang, J., Dou, X., Liu, Z., Andrew, R., Quinn, C. A., Poulter, B., Ouyang, Z., Yuan, W., Yuan, K., Zhu, Q., Li, F., Pan, N., Tian, H., Yu, X., Rocher-Ros, G., Johnson, M. S., Li, M., Li, M., Feng, D., Raymond, P., Yang, X., Canadell, J. G., Jackson, R. B., Yu, X., Li, Y., Saunois, M., Bousquet, P., and Peng, S.: Why methane surged in the atmosphere during the early 2020s, Science, 391, eadx8262, doi:10.1126/science.adx8262, 2026.

Liu, G., Shen, L., Ciais, P., Lin, X., Hauglustaine, D., Lan, X., Turner, A. J., Xi, Y., Zhu, Y., and Peng, S.: Trends in the seasonal amplitude of atmospheric methane, Nature, 641, 660-665, 10.1038/s41586-025-08900-8, 2025.

Peng, S., Lin, X., Thompson, R. L., Xi, Y., Liu, G., Hauglustaine, D., Lan, X., Poulter, B., Ramonet, M., Saunois, M., Yin, Y., Zhang, Z., Zheng, B., and Ciais, P.: Wetland emission and atmospheric sink changes explain methane growth in 2020, Nature, 612, 477-482, 10.1038/s41586-022-05447-w, 2022.